OPTIMIZATION AND TESTING OF A SUBSOILING BLADE FOR RUPTURING COMPACTED SOIL LAYERS USING THE DISCRETE ELEMENT METHOD
/
基于离散元法的破裂板结层深松铲优化设计与试验

He SUN, Xuan LUO, Tao WANG, Hongye LV, Haoran BAI*)
College of Mechanical and Electrical Engineering, Qingdao Agricultural University Qingdao /China
Tel: +86 13854285625; E-mail: baihaoran111@126.com
Corresponding author: Haoran BAI
DOI: https://doi.org/10.35633/inmateh-78-21

Keywords: *Sub-soiling shovel design, Discrete element method, Tillage resistance, Soil fragmentation rate, Saline-alkali soil improvement*

ABSTRACT
To address severe soil compaction, high draft resistance, and low subsoiling efficiency in saline-alkali soils, a soil-breaking subsoiling shovel aimed at reducing draft and enhancing soil comminution was designed. A discrete element method (DEM) soil model with graded particle sizes was established using the Hertz–Mindlin contact model with JKR (Johnson–Kendall–Roberts) adhesion. Simulation analyses were combined with an orthogonal experimental design to optimize the shovel's structural parameters and operating conditions. The optimal parameter combination—blade edge angle of 56.97°, blade inclination of 44.45°, and forward speed of 0.69 m·s⁻¹—resulted in a simulated draft of 2731.74 N and a maximum particle velocity of 2.75 m·s⁻¹. Field tests conducted at 0.69 m·s⁻¹ measured a draft of 2885.62 N, with a relative error of only 4.49% compared with the simulation, indicating high predictive reliability of the model. The mean soil comminution rate reached 57.79%, which is 64.5% higher than the conservation-tillage threshold (≥35%). These results demonstrate the usability and effectiveness of the proposed shovel. The optimized mechanical design reduces draft resistance while significantly improving soil fragmentation, and its overall operating performance meets the agronomic requirements for saline–alkali land improvement. Consequently, this design reduces energy consumption, enhances the soil environment for root growth, and exhibits strong agronomic applicability and environmental friendliness.

摘要
为解决盐碱土中土壤板结严重、牵引阻力高、深松效率低等问题，本文设计了一种破土型深松铲，旨在降低阻力并提高土壤碎土效果。基于离散元方法（DEM），采用 Hertz–Mindlin 接触模型结合 JKR(Johnson-Kendall-Roberts) 黏附建立分级粒径的盐碱土模型，并将仿真分析与正交试验设计相结合，优化深松铲的结构参数与作业条件。最优组合为：刃口角 56.97°、破土刀倾角 44.45°、前进速度 0.69 m·s⁻¹；在此条件下，仿真牵引阻力为 2731.74 N，颗粒最大流速 2.75 m·s⁻¹。田间试验在 0.69 m·s⁻¹ 下测得牵引阻力 2885.62 N，与仿真结果的相对误差为 4.49%，表明模型预测可靠。平均碎土率 57.79%，较保护性耕作阈值（≥35%）提高 64.5%。研究结果验证了所提深松铲的可用性与高效性：该机械设计可在显著降低牵引阻力的同时明显增强碎土效果，其总体作业性能满足盐碱地改良的农艺要求，为改善盐碱土结构提供了有效且具有创新性的技术方案。因此，该设计有助于降低耕作能耗，并为作物根系生长创造更有利的土壤环境，展现出良好的农艺适用性与环境友好性。

INTRODUCTION
Saline-alkali land is a very important land resource in China (*Zhang et al., 2024*). However, due to long-term erosion by soluble salts, the soil surface has accumulated serious salt, which has destroyed the soil structure. Under the action of cohesion, the soil surface has become hard, which has led to soil compaction (*Zhang & Wang, 2021*). This soil characteristic not only reduces the efficiency of water and nutrient utilization, but also significantly increases tillage resistance, making traditional machinery less adaptable in saline-alkali land (*Shao et al., 2019*). Deep tillage technology is widely used in soil cultivation (*Yuan et al., 2019*), deep loosening technology can break up the compacted layer, improve water utilization efficiency, and also has a desalination effect (*Zhuraev & Musulmanov, 2020*).

However, deep tillage operations require high-horsepower tractors for traction, which results in low operating efficiency and high tillage resistance. For severely compacted soils such as saline-alkali land, there is an urgent need to develop a low-resistance and high-efficiency deep tillage shovel to improve tillage quality, reduce energy consumption, and adapt to special operating environments such as saline-alkali land. This is not only of great significance for solving the problem of low quality of saline-alkali land farming, but also helps to promote the sustainable development of saline-alkali land agriculture and achieve the goals of high efficiency, high quality and low consumption in agricultural farming.

In view of the problems of large resistance and low efficiency during deep plowing operations using deep plowing shovels, researchers at home and abroad have conducted research from multiple angles. Shagholi et al. used a single-column chisel deep loosening shovel as the research object, and conducted a systematic study on the vibration frequency and vibration angle through a single-factor test method, and determined the optimal operating frequency and optimal vibration angle under specific test conditions (*Shahgoli et al., 2009, 2010*). Zhang Lei et al. designed a deep tillage shovel based on mole cricket bionics. They took the minimum sum of the inner and outer contour fitting errors as the optimal objective function, established an optimization model of the point cloud fitting function, and studied the effects of different tillage speeds on tillage performance, providing a theoretical reference for better selection of deep tillage working speed (*Zhang et al., 2022*). Sun Jianfeng et al. established a soil model of red soil and verified the feasibility of bionic deep tillage shovel in brick red soil (*Sun et al., 2020*). Li Jicheng and others used the discrete element method to analyze the soil movement changes during soil uplift, soil crushing and soil mixing, and found that the discrete element method can more accurately simulate the soil disturbance process in the soil (*Jicheng et al., 2023*). Qin Kuan and others explored the change and transmission of lateral force caused by double-wing deep tillers in sandy loam, analyzed the sinusoidal fluctuation law of deep tillers in shallow soil, middle soil and deep soil, and verified that the lateral force generated by deep tillage has the greatest impact on shallow soil (*Qin et al., 2022*). However, due to the special physical and chemical properties of saline-alkali land, deep plowing equipment designed for other soil types has poor adaptability. There are relatively few deep plowing and land preparation equipment that can be used for farming in saline-alkali land, and the operating efficiency and drag reduction performance still need to be improved. In addition, due to the serious soil compaction in saline-alkali land, the requirement for soil fragmentation rate is significantly higher than that of ordinary soil. It is hypothesized that optimizing the key geometric parameters of the blade based on discrete element method (DEM) simulations will significantly reduce the draft force of the subsoiling blade in saline–alkali soils and enhance its soil fragmentation performance.

In response to the properties of coastal saline–alkali soils, this study designs a soil-breaking deep-loosening shovel to reduce draft and enhance soil fragmentation. Using discrete element simulation in conjunction with experimental design and field testing, the stress state during blade–soil interaction is analyzed and the correlation between the shovel's deep-loosening performance and tillage resistance is elucidated. The findings provide key theoretical foundations and technical support for deep loosening and tillage operations in saline–alkali land. This study aims to optimize the structural and operational parameters of a soil-breaking subsoiling blade for saline–alkali soils using DEM-based simulations and field validation.

MATERIAL AND METHODS

Structural design of soil breaking and deep loosening shovel

During deep tillage, the handle of a traditional deep tillage shovel is in direct contact with the soil, and the handle is squeezed by the soil, so the handle is the main source of forward resistance (*Askari et al., 2019*; *Wang et al., 2023*). A soil-breaking blade is mounted at the tip of the deep-tillage shovel so that it engages the soil first. As the shovel advances, the blade crushes and compresses the soil, directing it laterally along both sides; consequently, the primary resistance otherwise acting on the shank is carried by the soil-breaking blade. Owing to its geometry, the blade effectively fractures compacted soil, markedly improving deep-tillage performance, lowering forward resistance, and increasing the degree of soil comminution. This configuration also reduces breakage and damage of the shovel itself.

According to the soil dynamics model, the main force - bearing parts of the soil - breaking and deep - tillage shovel are concentrated on the soil breaking knife, the deep - tillage shovel handle and the deep - tillage shovel tip (*Yang et al., 2023*).

The soil-breaking knife is mounted ahead of the deep-tillage shovel shank and is the primary source of tillage resistance. Placing it in front reduces draft and improves the soil-breaking rate. Following JB/T 9788–2020 (“Subsoiling Shovel and Subsoiling Shovel Handle”), a 3D model was built in which the assembly is split into a soil-breaking knife and a subsoiling shovel (Fig. 1). The knife’s role is to lower resistance during soil rupture. To ensure the strength of the soil breaking knife, the thickness of the soil breaking knife is designed to be B_1, the width of the soil breaking knife is B_2, the height of the soil breaking knife is H_2, the height of the subsoiling shovel is H_1, the edge angle of the soil breaking knife in contact with the soil is α, the inclination angle of the subsoiling shovel is σ, and the inclination angle of the soil breaking knife is β.

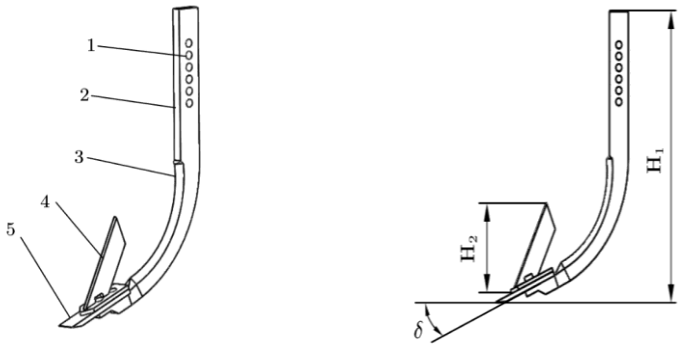

(a) Overall picture of the subsoiling blade with broken soil (b) Side view of broken ground subsoiling blade

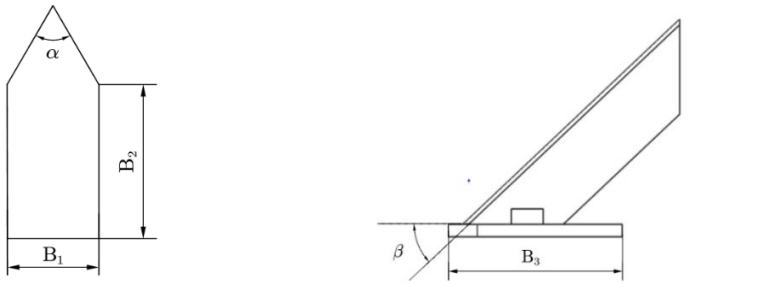

(c) *Cross-sectional view of the groundbreaker* (d) *Side view of the groundbreaker*

Fig. 1 - Schematic diagram of structural and geometric parameters

1. Installation hole; 2. Spare handle; 3. Shovel blade; 4. Break the ground knife; 5. Shovel tip

Force analysis of soil breaking and deep loosening shovel

When a soil-breaking and deep tilling shovel is used in deep tillage operations, the soil-breaking knife is in front of the shovel handle, so it is mainly affected by the force of the soil-breaking knife part and the shovel tip part. The force analysis of the subsoiling blade is performed by simplifying the contact model. As shown in Fig. 2, the total resistance force F_0 opposing the motion is generated by the interaction between the blade surface and the soil. To mathematically decompose the forces, the normal force and friction force are projected onto the horizontal direction.

Based on the equilibrium conditions and considering the symmetry of the blade, the force decomposition and the total resistance force F_0 are calculated as shown in Eqs. (1)-(3):

$$F_{edge-x} = N_1 \sin\left(\frac{\alpha}{2}\right) + \mu N_1 \cos\left(\frac{\alpha}{2}\right) \quad (1)$$

$$F_{side-x} = \mu N_2 \quad (2)$$

$$F_0 = 2\left(F_{edge-x} + F_{side-x}\right) = 2\left(N_1 \sin\left(\frac{\alpha}{2}\right) + \mu N_1 \cos\left(\frac{\alpha}{2}\right) + \mu N_2\right) \quad (3)$$

where:

F_0: resultant resistance force;

F_{edge-x}: horizontal resistance component acting on the cutting edge;

F_{side-x}: horizontal resistance component acting on the blade side surface;

N_1: normal force on cutting edge;

N_2: normal force on the shovel handle;

μ: soil-metal static friction coefficient;
α: cutting edge angle.

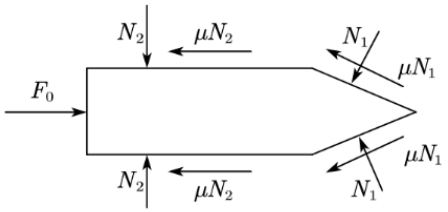

Fig. 2 - Analysis of the force on the blade of the deep-breaking earth blade

From Eq. (3), the total resistance F_0 depends on the blade angle α. On severely compacted saline–alkali soils, an inappropriate α increases draft. Thus, α must be chosen to reduce resistance while ensuring effective loosening: if α is too small, the loosened zone is inadequate; if too large, the enlarged soil–blade contact area raises resistance. Accordingly, the blade angle should be set with reference to the agricultural machinery design manual and tuned to saline–alkali soil characteristics to balance drag reduction and loosening efficiency.

During operation, the soil-breaking and deep-soiling shovel is mainly subjected to horizontal traction and the pressure of the soil on the soil-breaking blade and the shovel tip. The force conditions are shown in Fig. 3.

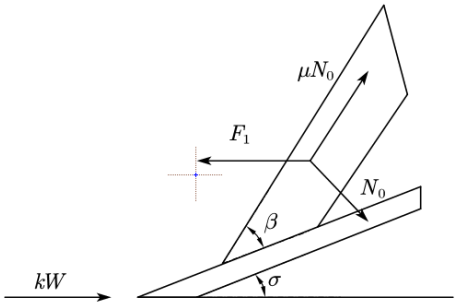

Fig. 3 - Analysis of the side stress of deep-breaking earth knife and shovel tip

Projecting normal and friction forces horizontally, the resistance components and total traction force F_1 are derived as Eqs. (4)-(6):

$$F_{tip-x} = N_0 \sin\sigma + \mu N_0 \cos\sigma \tag{4}$$

$$F_{blade-x} = N_2 \sin(\beta + \sigma) + \mu N_2 \cos(\beta + \sigma) \tag{5}$$

$$F_1 = F_{tip-x} + F_{blade-x} = N_0 \sin\sigma + \mu N_0 \cos\sigma + N_2 \sin(\beta + \sigma) + \mu N_2 \cos(\beta + \sigma) \tag{6}$$

where:

F_1: horizontal traction force on the tip;
F_{tip-x}: horizontal resistance component of the tip;
$F_{blade-x}$: horizontal resistance component of the soil-breaking blade;
N_0: positive pressure in the normal direction;
N_2: normal force on the shovel handle;
σ: subsoiling blade tip angle;
β: inclination angle of the groundbreaker;
μ: soil-metal static friction coefficient.

From (6), it can be seen that β and σ have a significant impact on the resistance of subsoiling blade, and they mainly act on the soil penetration performance and forward resistance of subsoiling blade. As the soil penetration angle increases, the soil penetration capacity gradually weakens and the resistance increases significantly. In addition, too large a soil penetration angle will also lead to poor soil loosening effect. Based on the special physical properties of saline-alkali land and combined with the agricultural machinery design manual, the soil penetration angle of the deep loosening shovel is designed, and the inclination angle σ of the deep loosening shovel tip is determined to be 23°. Through further experiments, the optimal value of the soil breaking knife inclination angle β is determined.

Establishment of a deep loose soil model for discrete saline-alkali land

Coastal saline-alkali land is an important soil resource in my country, but due to the influence of long-term salinization, the soil compaction phenomenon is serious. The soil layers of coastal saline-alkali land include the tillage layer, the compaction layer and the salt-rich layer, of which the vertical depth of the tillage layer is about 300 mm (*Wang et al., 2024*). Due to the particularity of saline - alkali land, in the process of deep tillage of saline - alkali land, it is necessary to ensure that the tillage operations do not damage the plow bottom layer of the saline - alkali soil, and at the same time, it is necessary to inhibit the salt from moving upward through the compacted layer. Therefore, for saline - alkali land cultivation, the tillage depth is usually no more than 300 mm. Sampling was carried out in the coastal saline-alkali land of Dongying City, Shandong Province, and the soil particle composition was shown in Table 1.

Table 1

Soil particle size distribution

Particle size /mm	Quality score
0~0.25	5
0.25~0.5	7.96
0.5~1	10.26
1~2	24.91
2~3	23.18
≥3	28.69

The saline–alkali soil is severely compacted, dominated by coarse particle sizes, and exhibits clear structural degradation. Deep loosening can markedly improve pore structure and the soil environment. Using the measured soil parameters, an EDEM 2022 tillage-layer model (300 mm depth) was built and virtual simulations of the soil-breaking subsoiling shovel were conducted.

Contact studies have shown that coastal saline - alkali soil is mainly composed of spherical particles of varying sizes. In EDEM software, the Hertz-Mindlin with JKR model can simulate the bonding and agglomeration effects of clay soil by assigning certain properties to the particle surface, and can also simulate the stress - strain characteristics of soil under particle stress conditions (*Kim et al., 2021*). Therefore, the Hertz-Mindlin with JKR model was selected as the soil simulation contact model. The three-dimensional model of the soil-breaking deep loosening shovel was established using SolidWorks, and the material used was 65# Mn steel. The contact parameters were obtained by experimental measurement and reference. The simulation intrinsic parameters of saline-alkali land are shown in Table 2.

Table 2

Discrete element soil calibration parameters

Parameter	Numeric
Soil particle density (kg/m^3)	2.270×10^3
Poisson's ratio of soil particles	0.32
Soil particle shear modulus (Pa)	1.20×10^{9}Pa
65Mn Density (Kg/m^3)	7.865×10^3
65Mn Poisson's ratio	0.30
65Mn shear modulus (Pa)	7.90×10^{9}Pa
Soil-Soil Recovery Coefficient	0.358
Soil-soil static friction coefficient	0.546
Soil-soil rolling friction coefficient	0.15
65Mn-Soil Recovery Coefficient	0.3
65Mn-Soil static friction coefficient	0.5
65Mn-Soil rolling friction coefficient	0.1
Gravity acceleration（m·s^{-2}）	9.81

The spherical structure was established using the particle unit provided by EDEM. The diameter of the soil particles used in the simulation was selected according to the soil particle size distribution and mass fraction (*He et al., 2024*). When setting the parameters of the soil particle factory, soil particles of different particle size ranges were generated according to the measured particle size above. The middle size of each interval was used as the actual simulation particle radius, and the particle factory within the same particle size range was evenly distributed to make the simulated soil closer to the actual soil particles (*Yan et al., 2022*). In order to balance the calculation time and the authenticity of the simulation results, the actual soil particle diameter was taken as 5 times the arithmetic mean and the two smaller particles were not included in the simulation for testing. The corresponding mass scores are shown in Table 3.

Table 3

Simulated particle diameter distribution

Simulated particle diameter / mm	Quality score / %
3.5	13.5
7.5	28.15
12.5	26.42
15	31.93

Soil particles were allowed to settle and accumulate to form a virtual soil trough representative of saline–alkali conditions. The trough measured 800 × 600 × 400 mm (L × W × H) with an actual soil height of 300 mm. The simulation model is shown in Fig. 4, with a tillage depth of 200 mm; the tillage process is shown in Fig. 5.

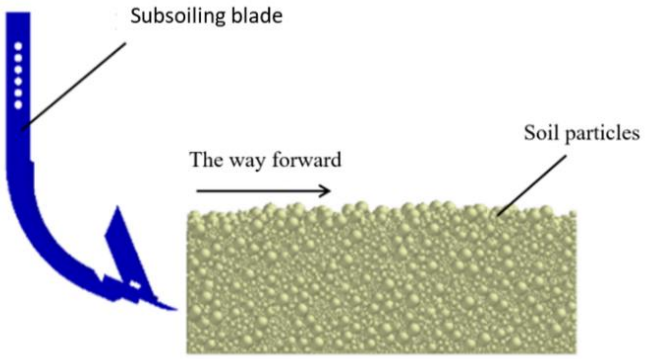

Fig. 4 - Simulated geometric model

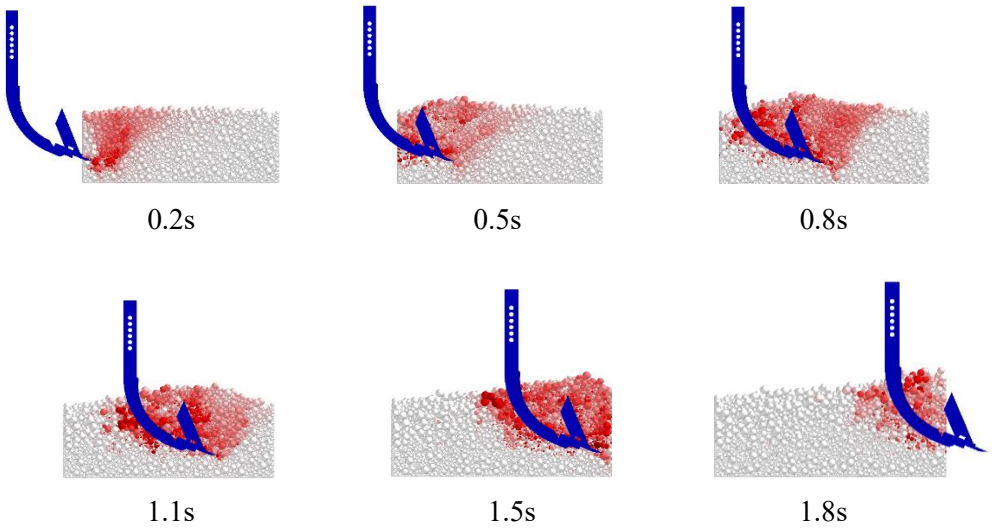

Fig. 5 - Effect diagram of interaction between subsoiling blade through soil breaking soil-soil particles

RESULTS AND DISCUSSIONS

Orthogonal test parameters

Guided by the tillage principle and simulation results, an orthogonal design was adopted with three primary factors: subsoiling speed 0.5–0.7 m·s^{-1}, blade angle 50–70°, and blade tilt 40–50°. These were coded as X_1 (speed), X_2 (blade angle), and X_3 (tilt) (Table 4). Using draft resistance (Y_1) and particle flow velocity (Y_2) as responses, the experiments were analyzed in Design-Expert, yielding effective regression equations for draft and soil fragmentation and an optimal parameter combination.

Table 4

Experimental factor level table

Level	Forward speed X_1/m·s-1	Cutting edge angle X_2/°	Ground breaking knife angleX_3/°
1	0.5	50°	40°
0	0.6	60°	45°
-1	0.7	70°	50°

Analysis of orthogonal test results

Orthogonal experimental design was performed using Design-Expert software, and 17 groups of experiments were generated. The experimental results are shown in Table 5.

Table 5

Simulation test results

Experiment No.	Forward speed	Cutting edge angle	Groundbreaking knife angle	Tillage resistance	Particle flow rate
	X_1 / m·s^{-1}	X_2 / °	X_3 / °	Y_1 / N	Y_2 / m·s^{-1}
1	0.6	60	45	2468.75	1.1313
2	0.6	70	50	2592.96	1.4253
3	0.5	60	40	2519.49	1.2306
4	0.7	50	45	3187.75	2.5874
5	0.6	60	45	2525.09	1.1253
6	0.5	60	50	2694.77	1.6494
7	0.6	60	45	2517.68	1.1315
8	0.5	50	45	2737.95	1.6106
9	0.5	70	45	3011.04	1.0248
10	0.7	70	45	3328.77	2.3462
11	0.6	60	45	2472.18	1.2253
12	0.6	50	40	2449.31	1.6513
13	0.7	60	40	3211.04	2.2702
14	0.6	50	50	2575.75	1.915
15	0.6	60	45	2298.65	1.2313
16	0.6	70	40	2549.17	1.1146
17	0.7	60	50	2891.99	2.7868

Establishment of regression equations and analysis of variance

Design-Expert software was used to perform regression analysis and fitting equation analysis on the test results. The variance analysis is shown in Table 6 and Table 7, respectively, where the p value < 0.05 indicates a significant effect.

Table 6

Variance analysis of tillage resistance regression model

Source	Sum of squares	Degrees of Freedom	Mean Square	F	P
Model	1.445E+06	9	1.605E+05	19.06	0.0004
X_1	3.429E+05	1	3.429E+05	40.72	0.0004
X_2	35269.02	1	35269.02	4.19	0.0799
X_3	87.52	1	87.52	0.0104	0.9217
X_1X_2	4360.62	1	4360.62	0.5178	0.4951
X_1X_3	61090.54	1	61090.54	7.25	0.0309
X_2X_3	1707.76	1	1707.76	0.2028	0.6661
X_1^2	8.478E+05	1	8.478E+05	100.67	< 0.0001
X_2^2	1.094E+05	1	1.094E+05	12.99	0.0087
X_3^2	24232.62	1	24232.88	2.88	0.1336
Residual	58951.01	7	8421.59		
Lack of Fit	25190.99	3	8397.00	0.9949	0.4807
Pure error term	33760.03	4	8440.03		
Total difference	1.504E+06	16			

Table 7

Analysis of variance of particle flow velocity regression model

Source	Sum of Squares	Degrees of Freedom	Mean Square	F	P
Model	5.13	9	0.5699	114.36	< 0.0001
X_1	2.50	1	2.50	502.34	< 0.0001
X_2	0.4294	1	0.4294	86.16	< 0.0001
X_3	0.2849	1	0.2849	57.18	0.0001
X_1X_2	0.0297	1	0.0297	5.96	0.0447
X_1X_3	0.0024	1	0.0024	0.4798	0.5108
X_2X_3	0.0006	1	0.0006	0.1108	0.7490
X_1^2	1.47	1	1.47	294.61	< 0.0001
X_2^2	0.0743	1	0.0743	14.90	0.0062
X_3^2	0.2128	1	0.2128	42.70	0.0003
Residual	0.0349	7	0.0050		
Lack of Fit	0.0231	3	0.0077	2.61	0.1882
Pure error term	0.0118	4	0.0029		
Total difference	5.16	16			

Note: X_1, X_2, X_3 are forward speed, cutting edge angle, and ground breaking knife inclination angle, respectively.

The analysis shows that for tillage resistance Y_1, operation speed X_1, X_1X_3, X_1^2, X_2^2 have significant effects on the test results, and the forward speed has a highly significant effect on tillage resistance. By analyzing the variance and removing the insignificant terms, the variance equation is (3).

$$Y_1 = 2456.47 + 207.04X_1 - 123.58X_1X_3 + 448.72X_1^2 + 161.19X_2^2 \quad (3)$$

For the particle flow velocity Y_2, the factors of forward speed X_1, X_2, X_3, X_1X_2, X_1^2, X_2^2, and X_3^2 have significant effects on the test results, while the other factors have no significant effects. The forward speed X_1 and the blade angle X_2 have extremely significant effects on the particle flow velocity. By performing variance analysis on them and removing the insignificant terms, the regression equation (4) is obtained.

$$Y_2 = 1.17 + 0.5594X_1 + 0.2317X_2 + 0.1887X_3 + 0.0862X_1X_2 + 0.5905X_1^2 + 0.1328X_2^2 + 0.2248X_3^2 \quad (4)$$

Influence of Factor Interactions on Operational Performance

The draft-resistance response surface (Fig. 6) shows that resistance rises with forward speed. Blade angle exhibits a non-monotonic effect: as the angle first increases, optimized cutting improves efficiency and lowers unnecessary friction, producing a slight decline in resistance; with further increases, cutting efficiency weakens, blade–soil contact area grows, friction rises, and resistance increases. Forward speed exerts the strongest influence—greater speed intensifies soil disturbance and cutting, thereby increasing resistance.

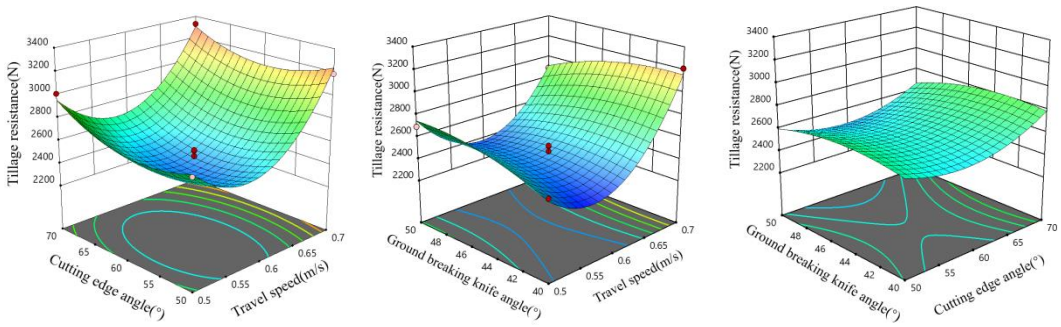

Fig. 6 - Response surface of tillage resistance

The particle flow–velocity response surface (Fig. 7) shows a clear speed effect: as forward speed increases, blade–soil interaction intensifies, producing higher disturbance and shear per unit time and thus markedly increasing particle velocity. Blade angle also has a pronounced, non-linear influence—by altering cutting and crushing efficiency and the stress state of soil particles, it modulates flow; within an optimized angle range, particle motion is promoted and operating efficiency improves. In addition, the blade inclination is an important factor: changing the inclination alters the direction and magnitude of forces on particles, affecting their trajectories and velocities.

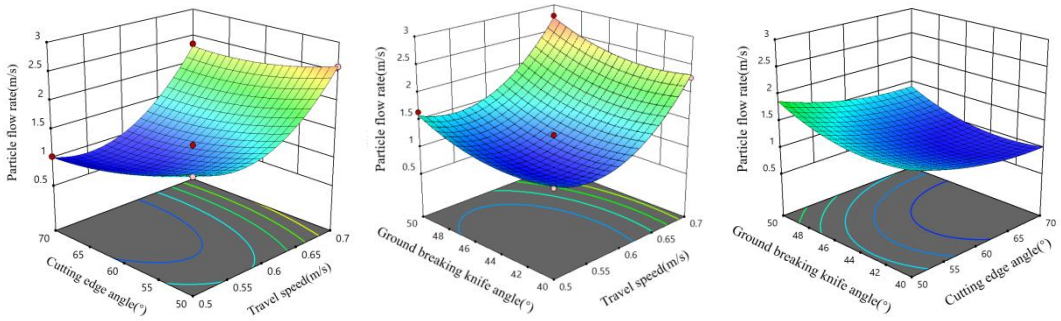

Fig. 7 - Response surface of particle flow velocity

Taking tillage resistance and particle flow velocity as the optimization objectives, the regression model was analyzed and solved using Design-Expert software. After optimization, the optimal parameter combination was obtained: when the forward speed is 0.69 m·s^{-1}, the edge angle is 56.97°, and the soil-breaking blade angle is 44.45°, the tillage resistance is 2761.74 N, and the maximum particle flow velocity is 2.75 m·s^{-1}.

Field trial

In order to test the actual operation effect of the soil-breaking deep tillage shovel and verify the simulation result analysis of the deep tillage shovel, a field test was carried out on the deep tillage shovel to obtain the actual deep tillage effect.

In order to test the reliability of the structural parameters of the soil - breaking deep tillage shovel, a field test was conducted in the saline - alkali land test field in Dongying Agricultural High - tech Zone.

The moisture content of the test field was 12.39%. The test equipment included a chisel deep tillage shovel, a soil - breaking deep tillage shovel, an Ouqi XSD1604 tractor, a deep tillage and fertilizer spreader frame, a meter ruler, and a soil pick. The test field was a coastal saline - alkali land, and the field test setup is shown in Fig. 8.

Fig. 8 - Schematic diagram of field experiment

The deep tillage frame is connected to the tractor's three-point suspension to ensure the smooth operation of the machine. During the test, the machine travels 100 m each time (20 m in the preparation area, 60 m in the test area, and 20 m in the adjustment area), and the test is repeated 10 times. The tillage depth of the test area is set to 200 mm, and the forward speed of the tractor is set to 0.69 $m \cdot s^{-1}$.

The soil crushing rate index was measured with reference to the national standard of China for conservation tillage machinery: deep loosening shovel (standard number: GB/T 24675.2-2024). The rated operating speed was used for two round trips, one point was measured in each row, and samples were taken along the tillage direction. The test was repeated 10 times.

According to the deep tillage operation standard, the soil in the test area was excavated and collected, and the total mass of the soil blocks was measured to be G (kg). The weight of the soil blocks not larger than 4 cm was G_S (kg). The soil crushing rate was considered qualified when it was measured to be greater than 35%. The calculation formula is (5).

$$C = \frac{G_S}{G} \times 100\% \quad (5)$$

During the field test, the soil crushing effect was good, the deep loosening shovel operation was stable, and there was no clay phenomenon. Through the test data processing, the average value of 10 times was obtained using Excel software, and the tillage resistance was 2885.62 N, with a relative error of 4.49% from the expected result, and the soil crushing rate was 57.79%, which was 64.54% higher than the threshold (≥35%) specified in the national standard for conservation tillage machinery.

CONCLUSIONS

This study targets the practical challenges of saline–alkali compacted topsoil-difficult rupture, high draft, and low efficiency-and investigates the design optimization and operating mechanisms of a soil-breaking subsoiling blade. A DEM soil model using the Hertz-Mindlin with JKR contact (calibrated to measured soil properties) was constructed. Combined with simulations and an orthogonal experimental design, the effects of edge angle, blade inclination, and forward speed on draft/cutting forces and soil comminution were systematically evaluated. At the design level, a parameterized design guideline was proposed in which the triad “edge angle–inclination–speed” cooperatively governs crack initiation and propagation, thereby forming a reusable geometric design framework for subsoiling blades.

Results show an optimal combination of edge angle 56.97°, blade inclination 44.45°, and forward speed 0.69 $m \cdot s^{-1}$. Under this setup, the simulated draft force was 2731.74N, and the field-measured value was 2885.62 N (relative error 4.49%), indicating credible model predictions; the maximum particle velocity reached 2.75 $m \cdot s^{-1}$, and the soil comminution rate averaged 57.79%, which is 64.5% higher than the agronomic threshold for conservation tillage (≥35%). The compacted layer was effectively ruptured and loosened while reducing draft and maintaining work quality. The study provides quantitative evidence for the coupled optimization of geometry and operating parameters of soil-breaking subsoiling blades and shows good scalability to cohesive/high-strength soils. Future research will focus on the interaction mechanism of multi-blade systems and conduct an in-depth analysis of field energy consumption to further improve the operational efficiency of subsoiling tillage in saline–alkali lands.

ACKNOWLEDGEMENT

This work was supported by National Key Research and Development Program of China (Project no. 2023YFD2001400), National Key R&D Program of China (Project no.2022YFE0125800).

REFERENCES

[1] Askari, M., Shahgholi, G., & Abbaspour-Gilandeh, Y. (2019). New wings on the interaction between conventional subsoiler and paraplow tines with the soil: effects on the draft and the properties of soil. *Archives of Agronomy and Soil Science*, 65(1), 88–100. https://doi.org/10.1080/03650340.2018.1486030

[2] He, X., Ma, S., Liu, Z., Wang, D., Shang, S., Li, G., & Li, H. (2024). Calibration and testing of saline soil parameters based on edem discrete element methodology. *INMATEH Agricultural Engineering*, 822–833. https://doi.org/10.35633/inmateh-73-69

[3] Jicheng, L., Kunpeng, S., Yonghua, Z., & Tianhui, Z. (2023). Simulation of Tillage Behavior of Double Winged Subsoiler Based on Discrete Element Method. *Journal of Inner Mongolia Agricultural University* (Natural Science Edition), 44(2), 67-75.

[4] Kim, Y.-S., Siddique, Md. A. A., Kim, W.-S., Kim, Y.-J., Lee, S.-D., Lee, D.-K., Hwang, S.-J., Nam, J.-S., Park, S.-U., & Lim, R.-G. (2021). DEM simulation for draft force prediction of moldboard plow according to the tillage depth in cohesive soil. *Computers and Electronics in Agriculture*, 189, 106368. https://doi.org/10.1016/j.compag.2021.106368

[5] Qin, K., Zhao, Y., Zhang, Y., Cao, C., & Shen, Z. (2022). Lateral stress and its transmission law caused by operation of a double-wing subsoiler in sandy loam soil. *Frontiers in Environmental Science*, 10. https://doi.org/10.3389/fenvs.2022.986361

[6] Shahgoli, G., Fielke, J., Desbiolles, J., & Saunders, C. (2010). Optimising oscillation frequency in oscillatory tillage. *Soil and Tillage Research*, 106(2), 202–210. https://doi.org/10.1016/j.still.2009.10.005

[7] Shahgoli, G., Saunders, C., Desbiolles, J., & Fielke, J. (2009). The effect of oscillation angle on the performance of oscillatory tillage. *Soil and Tillage Research*, 104(1), 97–105. https://doi.org/10.1016/j.still.2009.01.003

[8] Shao, H., Chu, L., Lu, H., Qi, W., Chen, X., Liu, J., Kuang, S., Tang, B., & Wong, V. (2019). Towards sustainable agriculture for the salt-affected soil. *Land Degradation & Development*, 30(5), 574–579. https://doi.org/10.1002/ldr.3218

[9] Sun, J., Chen, H., Wang, Z., Ou, Z., Yang, Z., liu, Z., & Duan, J. (2020). Study on plowing performance of EDEM low-resistance animal bionic device based on red soil. *Soil and Tillage Research*, 196, 104336. https://doi.org/10.1016/j.still.2019.104336

[10] Wang, D., Tong, L. U., Zhuang, Z., Shang, S., Shuai, Z., & Liu, J. (2024). Calibration of Discrete Element Simulation Parameters for Cultivated Soil Layer in Coastal Saline alkali Soil. (滨海盐碱地耕作层土壤离散元仿真参数标定方法) https://link.cnki.net/urlid/11.1964.S.20240903.1531.002

[11] Wang, J., Feng, W., Zhang, H., Sun, J., & Zhao, Q. (2023). Drag Reduction Method of Deep Pine Components in Soda Saline-Alkali Soil for a Smart City. *Journal of Testing and Evaluation*, 51(3), 1461–1477. https://doi.org/10.1520/JTE20220125

[12] Yan, D., Yu, J., Wang, Y., Zhou, L., Tian, Y., & Zhang, N. (2022). Soil Particle Modeling and Parameter Calibration Based on Discrete Element Method. *Agriculture*, 12(9), 1421. https://doi.org/10.3390/agriculture12091421

[13] Yang, W., Xiao, X., Pan, R., Guo, S., & Yang, J. (2023). Numerical Simulation of Spiral Cutter–Soil Interaction in Deep Vertical Rotary Tillage. *Agriculture*, 13(9), 1850. https://doi.org/10.3390/agriculture13091850

[14] Yuan, J., Feng, W., Jiang, X., & Wang, J. (2019). Saline-alkali migration in soda saline soil based on sub-soiling technology. *Desalination and Water Treatment*, 149, 352–362. https://doi.org/10.5004/dwt.2019.23856

[15] Zhang, B., & Wang, N. (2021). Study on the Harm of Saline Alkali Land and Its Improvement Technology in China. *IOP Conference Series: Earth and Environmental Science*, 692(4), 042053. https://doi.org/10.1088/1755-1315/692/4/042053

[16] Zhang, G., Bai, J., Zhai, Y., Jia, J., Zhao, Q., Wang, W., & Hu, X. (2024). Microbial diversity and functions in saline soils: A review from a biogeochemical perspective. *Journal of Advanced Research*, 59, 129–140. https://doi.org/10.1016/j.jare.2023.06.015

[17] Zhang, L., Zhai, Y., Chen, J., Zhang, Z., & Huang, S. (2022). Optimization design and performance study of a subsoiler underlying the tea garden subsoiling mechanism based on bionics and EDEM. *Soil and Tillage Research*, 220, 105375. https://doi.org/10.1016/J.STILL.2022.105375

[18] Zhuraev, F.U., & Musulmanov, F. Sh. (2020). Equipment and Technology Application for Washing Highly Saline Soils. *Agricultural Machinery and Technologies*, 14(2), 29–33. https://doi.org/10.22314/2073-7599-2020-14-2-29-33